Journal of Electroceramics, 13, 229–233, 2004

Annealing Effects on Structural and Dielectric Properties of Tunable BZT Thin Films

JIN XU,* WOLFGANG MENESKLOU & ELLEN IVERS-TIFFÉE
Institut für Werkstoffe der Elektrotechnik, Universität Karlsruhe (TH), 76131 Karlsruhe, Germany

Submitted February 14, 2003; Revised February 18, 2004; Accepted February 19, 2004

Abstract. $Ba(Zr,Ti)O_3$ thin films have attracted great attention in recent years for their potential use in DRAMs and MCMs due to their high dielectric constant and relatively low leakage current. However, their tunable dielectric properties were rarely investigated and the corresponding potential for tunable microwave applications was seldom reported.

In this paper, we present the tunable dielectric behavior of BZT thin films deposited by RF magnetron sputtering from a $Ba(Zr_{0.3}Ti_{0.7})O_3$ ceramic target on MgO single crystal substrates. The composition, thickness and crystallinity of the thin films were analyzed by Rutherford backscattering (RBS), scanning electron microscopy (SEM) and X-ray diffraction (XRD), respectively. The dielectric constant and loss tangent were measured as a function of electric field (0–7 kV/mm) and temperature (-140 to $+160^{\circ}$C) at frequencies up to 1 MHz, using interdigital capacitors (IDC) with Au electrodes on thin films. By optimizing the preparation process, a tunability {defined as $\tau = [\varepsilon(0) - \varepsilon(E_{\max})]/\varepsilon(0)$} of 76% at $E_{\max} = 7$ kV/mm and a low loss tangent of 0.0078 can be achieved. In addition, the influence of annealing temperature on the dielectric properties of the thin films is also discussed.

Keywords: $Ba(Zr,Ti)O_3$, thin films, tunable dielectric properties, RF sputtering

1. Introduction

Some ferroelectric materials with perovskite structure (e.g. $Ba_xSr_{1-x}TiO_3$) are prospective candidates for microwave applications [1, 2], due to the reasons of high dielectric nonlinearity (manifested as the dependence of dielectric constant on electric field) and relatively low losses. Concerning both the commercial and military applications, in the coming future, many tunable microwave components such as tunable oscillators, tunable filters, phase shifters and varactors [3–5] will be realized for wireless communications and satellite applications. For example, for the aim of automobile driving assistance, scanning radars using phase shifters fabricated by tunable materials could be equipped into the collision warning systems of cars.

In recent years, a considerable amount of research work has been done in the area of developing tunable ferroelectric thin films for matching the increasing requirements of high performance electric field tunable microwave devices. Commonly, the studies in this field are mainly focused on the $Ba_xSr_{1-x}TiO_3$ (BST) system [3–7]. Regardless of deposition method and substrate type, the critical properties of the thin films which need to be optimized are the magnitude of tunability as a function of applied electric field and dielectric losses.

In the last few years, $Ba(Zr,Ti)O_3$ (BZT) thin films have attracted much attention for dynamic random access memory (DRAM) [8, 9] multi-chip modules (MCMs) [10], and capacitors [11] applications, due to their high dielectric constant and relatively low leakage current. However, their tunable dielectric properties were rarely investigated.

In our former work, the temperature dependence of dielectric properties was investigated for $Ba(Zr_xTi_{1-x})O_3$ ($x = 0.25, 0.30$) thick films with applied electric field at low frequencies [12, 13]. In contrast to bulk ceramics, much lower dielectric

*To whom all correspondence should be addressed. E-mail: jin.xu@iwe.uni-karlsruhe.de

permittivity and a more diffused phase transition were observed for BZT thick films. A tunability of 26% was achieved for a $Ba(Zr_{0.25}Ti_{0.75})O_3$ thick film at $E_{max} = 2$ kV/mm, measured at 20 kHz and room temperature (RT) [12], while a $Ba(Zr_{0.3}Ti_{0.7})O_3$ thick film exhibited $\tau = 16\%$ at $E_{max} = 4$ kV/mm, 1 MHz and RT [13].

In this paper, we present the tunable dielectric behavior of BZT thin films deposited by RF magnetron sputtering from a $Ba(Zr_{0.3}Ti_{0.7})O_3$ ceramic target on MgO single crystal substrates. The composition, thickness and crystallinity of the thin films were characterized. The temperature dependence of dielectric constant and loss tangent was measured as a function of electric field at frequencies up to 1 MHz, using interdigital capacitors (IDC) with Au electrodes on thin films. The effect of post-annealing on the dielectric properties of BZT thin films has been investigated, and the results and discussion are focused on the influence of the annealing temperature.

2. Experimental

A sintered stoichiometric $BaZr_{0.3}Ti_{0.7}O_3$ ceramic disk with a diameter of 100 mm was used as target. BZT thin films with a thickness of 190 nm were deposited on (100) MgO single crystal substrates by RF magnetron sputtering. The substrates were positioned 35 mm oppositely away from the target ("on-axis" sputtering). Thin films were prepared at a substrate temperature (T_S) of 650°C, using an Ar–O_2 gas mixture, at a total pressure of 5.5×10^{-2} mbar. The sputtering conditions are listed in Table 1.

In our former studies on BST thin films [14], it was found that the tunability of the samples can be significantly increased by post-annealing in air at 900°C for 5 hours. Therefore, a post-annealing process has also been conducted for BZT films. In order to study the influence of the annealing temperature (T_A), the samples were annealed in air at different temperatures (650, 900 and 1100°C) for 5 hours, with a heating and cooling rate of 5 K/min.

Table 1. Sputtering conditions of BZT thin films.

Target-Substrate distance	35 mm
Substrate temperature	650°C
Sputtering gas	O_2:Ar = 10 sccm:90 sccm
Total pressure of sputtering gas	5.5×10^{-2} mbar
Plasma power	RF 150 W
Deposition time	60 min

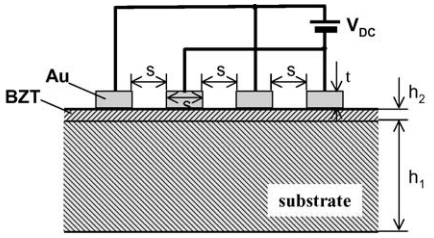

h_1 = 500 µm (substrate), h_2 = 190 nm (BZT), s = 20 µm, t = 100 nm.

Fig. 1. Cross-section structure of IDC.

The composition of the BZT thin films was determined by Rutherford backscattering (RBS). Thin film surface, cross-section microstructures and the thickness were observed using scanning electron microscopy (SEM) (LEO1530). The crystallographic structure and orientation of BZT thin films were analyzed using X-ray diffraction (XRD) (Siemens D5000, Cu K_α radiation).

The dielectric properties (dielectric constant ε_r, loss tangent $\tan\delta$ and tunability τ) of BZT thin films were measured as a function of applied electric field (0–7 kV/mm) and temperature (−140°C to +160°C) at low frequencies (≤1 MHz), using an ALPHA-H high-resolution dielectric analyzer (NOVOCONTROL). To obtain the values of ε_r and $\tan\delta$, capacitance and loss measurements of interdigital capacitors (IDC) were carried out, as described in [15]. The IDC, as shown in Fig. 1, were fabricated on BZT thin film by sputtering a 10 nm chromium adhesion film and a 100 nm thick gold layer, followed by a standard lift-off process. A modified conformal mapping technique and a partial capacitance method were applied to evaluate the dielectric properties [16].

3. Results and Discussion

3.1. Characterization of As-Deposited BZT Thin Films

From the XRD θ-2θ scan pattern shown in Fig. 2, it is clear that the as-deposited BZT thin film is single-phase and highly c-axis oriented.

The typical film compositions determined by RBS (5–10% deviation of evaluation) were relatively

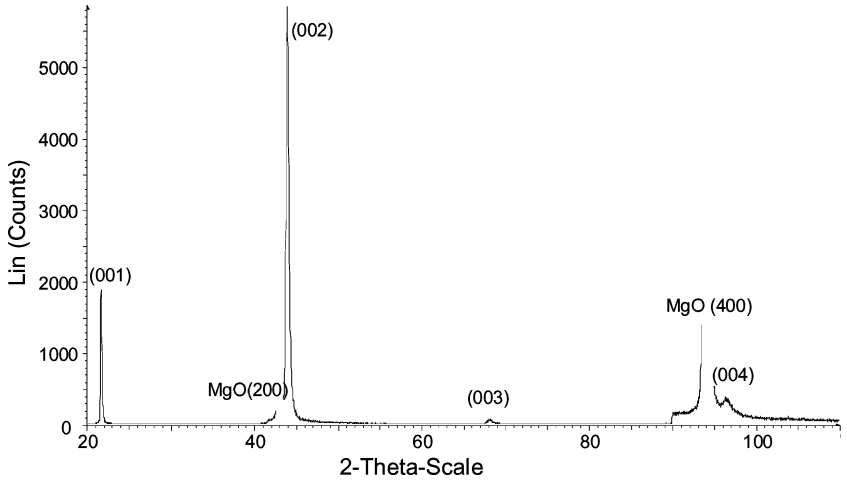

Fig. 2. XRD pattern of as-deposited BZT thin film.

constant, as $BaZr_xTi_yO_{3-\delta}$ ($x = 0.26$–0.31; $y = 0.72$–0.79), and indicated the proper composition of the films.

Observed from the SEM micrographs, the surface of the as-deposited film is extremely smooth and homogeneous. A thickness of 190 nm for the thin film was determined from the cross-section micrograph, and the growth rate of the thin film was calculated to be about 3.17 nm/min.

3.2. *XRD Analyses of Annealed BZT Thin Films*

The XRD analysis of θ-2θ scan and ω-scan were carried out for BZT thin films annealed in air for 5 hours at different temperatures. The analytic data are shown in Table 2.

From the θ–2θ scan patterns, it is observed that all the samples are still single-phase and exclusively (00l) orientated. The out-of-plane lattice constant (c) can be calculated from the position of the BZT (002) peak. Note that with higher T_A, the c value decreases and approaches the value of the bulk material ($c_{\text{bulk}} = 4.06$ Å for $Ba(Zr_{0.3}Ti_{0.7})O_3$).

Table 2. XRD analytic data of various BZT thin films annealed at different temperatures.

	Samples annealed at different temperatures		
XRD analysis data	650°C	900°C	1100°C
θ–2θ scan 2θ cal. c (Å)			
	44.16°	44.46°	44.62°
	4.10	4.07	4.06
ω-scan of (002) peak ω FWHM			
	22.10°	22.23°	22.32°
	0.34°	0.24°	0.23°

The full width at half maximum (FWHM) values of the ω-scan peak for BZT (002) reflection were determined as 0.34°, 0.24° and 0.23°, respectively, which indicates a better out-of-plane orientation appearing with the increasing of T_A.

For θ-2θ scan of XRD, the diffraction line broadening due to the effects of internal film strain and crystallite size can be separated from each other, by means of Halder and Wagner plots [17, 18], where $\Delta^2(2\theta)/\tan^2\theta$ is plotted versus $\Delta(2\theta)/(\tan\theta \sin\theta)$. This estimation is on the basis of the following equation that leads to numerical solutions for internal strain (e) and mean value of small crystallite size (L), expressed as [19].

$$\frac{\Delta^2(2\theta)}{\tan^2\theta} = \frac{K\lambda}{L}\left(\frac{\Delta(2\theta)}{\tan\theta \sin\theta}\right) + 16e^2$$

where $\Delta(2\theta)$ means the full width at half maximum in 2θ of (00l) reflections; K is the so-called "shape-factor" which usually takes a value of 0.9 [19].

From such plots straight lines are obtained whose slope yields the mean crystallite size and whose axial section yields the strain.

In Fig. 3, the data for as-deposited and annealed BZT thin film are shown. From the respective "linear fits", the values of internal strain (e) and mean crystallite size (L) were estimated, as shown in Table 3.

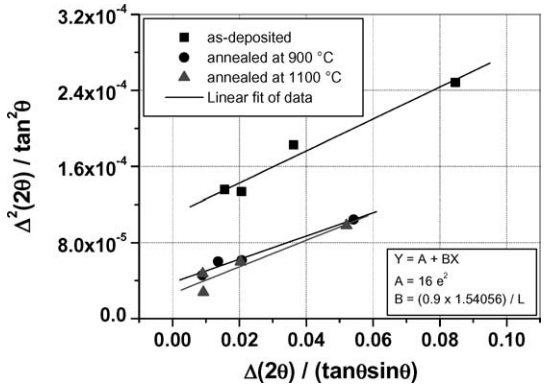

Fig. 3. Plots after Halder and Wagner for estimating the internal film strain. The data are shown for as-deposited and annealed (at 900 and 1100°C) BZT thin films.

	Samples		
Estimated data	As-deposited $T_S = 650$°C	Annealed at $T_A = 900$°C	Annealed at $T_A = 1100$°C
e (internal strain)	0.26%	0.15%	0.13%
L (mean cryst. size)	∼825 Å	∼1136 Å	∼990 Å

Table 3. Estimated data of as-deposited and annealed BZT thin films.

It can be seen that the internal strain values of the annealed samples are smaller in comparison to that of the as-deposited sample, indicating that the stress in the thin film has been released after annealing, further at higher temperature. Moreover, the mean crystallite size of the annealed sample is larger than that of the as-deposited one, which reveals the regrowth of the grains in the thin film induced by high temperature. Here the shown mean crystallite size of 1100°C annealed sample is a little smaller than that of the sample annealed at 900°C, which might caused by the error of the data estimation.

3.3. *Dielectric Properties*

The dielectric constant (ε_r) and loss tangent (tanδ) as a function of the temperature for BZT thin films annealed at different temperatures are plotted in Fig. 4. It is obvious that for the sample annealed at 1100°C, the dielectric constant (ε_r) shows a much higher temperature dependence, as well as much higher values than those of the samples annealed at 900°C and 650°C (e.g., 2437 versus 592 and 395 at room temperature, respectively).

Furthermore, the temperature of maximum permittivity $T_{\max}$ is shifted to around 233 K, i.e. 60 K higher in comparison to the 173 K of the sample annealed at 900°C. Correspondingly, the loss tangent of the sample annealed at 1100°C increases rapidly with decreasing temperature, while for the other two samples the losses remain at a low level.

By measuring the bias dependence of dielectric constants, the tunability can be calculated and plotted as a function of the temperature, as shown in Fig. 5. It is noteworthy that the sample annealed at 1100°C shows a significant high tunability of 76% at room temperature, which is much higher than that of the sample annealed at 900°C (about 12%). The sample

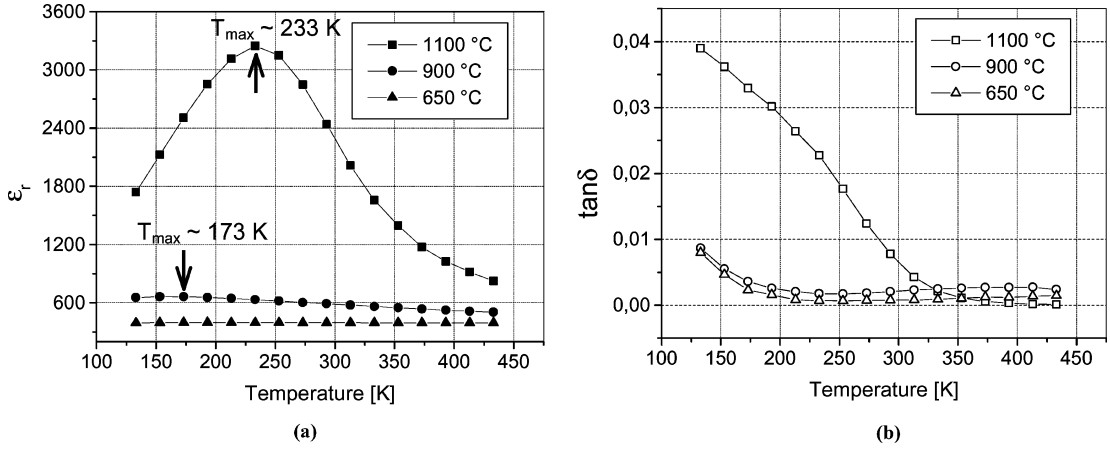

Fig. 4. Temperature dependence of (a) dielectric constant (ε_r), and (b) loss tangent (tanδ) of BZT thin films annealed at different temperatures, measured at 1 kHz.

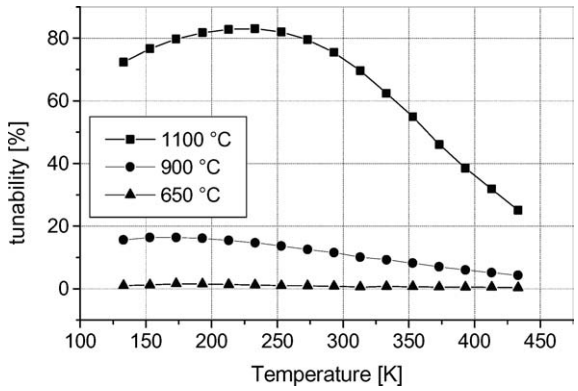

Fig. 5. Temperature dependence of tunability for BZT thin films annealed at different temperatures, measured at 1 kHz.

annealed at 650°C shows only a tunability close to zero, which is similar to that of the as-deposited sample.

Correlating the crystal structure to the dielectric properties, the crystallinity of the thin film is improved by increasing the annealing temperature up to 1100°C; as a consequence the dielectric permittivity increases. In addition, the as-deposited thin films are highly stressed, whereas the stress of the film was released after annealing, which may result in a shift of maximum dielectric permittivity. For the thin film with better crystallinity, higher tunability and higher losses occurred around the point of maximum permittivity ($T_{\max}$).

4. Summary

The microstructure and dielectric properties of RF sputtered BZT thin films influenced by post-annealing were investigated. Tunability can be significantly increased by increasing the annealing temperature. A tunability of 76% at $E_{\max} = 7$ kV/mm and a loss tangent of 0.0078 have been achieved for a sample annealed at 1100°C, measured at 1 kHz and room temperature. The improvement of the crystallinity and the release of the stress after annealing are dominant factors which pronouncedly affect the dielectric properties of the annealed BZT thin films.

Acknowledgments

The authors acknowledge Dr. D. Fuchs and Dr. R. Fromknecht at the Research Center of Karlsruhe (FZK), for the helpful discussions and their help in XRD and RBS analyses of the thin film samples, respectively. The authors would like to thank Prof. Dr. M. Siegel and A. Stassen from the IMS, Universität Karlsruhe (TH), for technical support. Further thanks go to F. Zimmermann and M. Voigts for the measurement assistance.

This work was supported by the BMBF, PTJ-NMT #03N10574.

References

1. V.K. Varadan and V.V. Varadan, *Proceedings of SPIE*, **2448**, 35 (1995).
2. F. Zimmermann, J. Xu, M. Voigts, W. Menesklou, and E. Ivers-Tiffée, *Proceedings of Materials Week 2000*.
3. J.M. Pond, S.W. Kirchoefer, W. Chang, J.S. Horwitz, and D.B. Chrisey, *Intergr. Ferroelectr.*, **22**, 317 (1998).
4. Im. Jaemo, O. Auciello, P.K. Baumann, S.K. Streiffer, D.Y. Kaufman, and A.R. Krauss, *Appl. Phys. Lett.*, **76**, 625 (2000).
5. J.D. Baniecki, R.B. Laibowitz, T.M. Shaw, P.R. Duncombe, D.A. Neumayer, D.E. Kotecki, H. Shen, and Q.Y. Ma, *Appl. Phys. Lett.*, **72**, 498 (1998).
6. W.T. Chang, J.S. Horwitz, W.J. Kim, J.M. Pond, S.W. Kirchoefer, C.M. Gilmore, S.B. Qadri, and D.B. Chrisey, *Intergr. Ferroelectr.*, **24**, 257 (1999).
7. C.L. Chen, H.H. Feng, Z. Zhang, A. Brazdeikis, Z.J. Huang, W.K. Chu, and C.W. Chu, *Appl. Phys. Lett.*, **75**, 412 (1999).
8. T.B. Wu, C.M. Wu, and M.L. Chen, *Appl. Phys. Lett.*, **69**, 2659 (1996).
9. J.H. Lee, T.S. Chen, V. Balu, J. Han, R.M. Ali, S. Gopalan, C.H. Wong, and J.C. Lee, *Mater. Res. Soc*., Ferroelectric thin films VII symposium, 47 (1999).
10. N. Kamehara, M. Tsukada, J.S. Cross, and K. Kurihara, *J. Ceram. Soc. Jpn.*, **105**, 746 (1997).
11. U. Weber, G. Greuel, U. Boettger, S. Weber, D. Hennings, and R. Waser, *J. Am. Ceram. Soc.*, **84**, 759 (2001).
12. M. Voigts, W. Menesklou, and E. Ivers-Tiffée, *Intergr. Ferroelectr.*, **39**, 383 (2001).
13. M. Voigts, F. Zimmermann, J. Xu, W. Menesklou, and E. Ivers-Tiffée, *Proceedings of Materials Week 2002*.
14. J. Xu, W. Menesklou, and E. Ivers-Tiffée, to be published in *J. European Ceram. Soc.,* **24**, 1735 (2004).
15. C. Weil, P. Wang, H. Downar, J. Wenger, and R. Jakoby, *Frequenz*, **54**, 250 (2000).
16. S.S. Gevorgian, T. Martinsson, P.L.J. Linnér, and E.L. Kollberg, *IEEE Trans. Microwave Theory Tech.*, **44**, 896 (1996).
17. N.C. Halder and C.N.J. Wagner, *Acta Crystallogr*., **20**, 312 (1966).
18. D. Fuchs, M. Adam, P. Schweiss, S. Gerhold, S. Schuppler, and R. Schneider, *J. Appl. Phys*., **88**, 1844 (2000).
19. H.P. Klug and L.E. Alexander, *X-ray Diffraction Procedures*, 2nd ed. (Wiley, NewYork, 1974), pp. 656–665.